Geosci. Model Dev., 7, 2077–2090, 2014
www.geosci-model-dev.net/7/2077/2014/
doi:10.5194/gmd-7-2077-2014

Geoscientific Model Development
Open Access

A suite of early Eocene (∼ 55 Ma) climate model boundary conditions

N. Herold[1], J. Buzan[2], M. Seton[3], A. Goldner[2], J. A. M. Green[4], R. D. Müller[3], P. Markwick[5], and M. Huber[1,6]

[1]Earth Systems Research Center, Institute for Earth, Ocean and Space Sciences, University of New Hampshire, Durham, NH, USA
[2]Department of Earth, Atmosphere, Planetary and Space Sciences, Purdue University, West Lafayette, IN, USA
[3]EarthByte Group, School of Geosciences, University of Sydney, Sydney NSW, Australia
[4]School of Ocean Sciences, Bangor University, Menai Bridge, UK
[5]Getech, Leeds, LS8 2LJ, UK
[6]Department of Earth Sciences, University of New Hampshire, Durham, NH, USA

Correspondence to: M. Huber (matthew.huber@unh.edu)

Received: 14 December 2013 – Published in Geosci. Model Dev. Discuss.: 17 January 2014
Revised: 27 April 2014 – Accepted: 3 July 2014 – Published: 16 September 2014

Abstract. We describe a set of early Eocene (∼ 55 Ma) climate model boundary conditions constructed in a self-consistent reference frame and incorporating recent data and methodologies. Given the growing need for uniform experimental design within the Eocene climate modelling community and the challenges faced in simulating the prominent features of Eocene climate, we make publicly available our data sets of Eocene topography, bathymetry, tidal dissipation, vegetation, aerosol distributions and river runoff. Major improvements in our boundary conditions over previous efforts include the implementation of the ANTscape palaeotopography of Antarctica, more accurate representations of the Drake Passage and Tasman Gateway, as well as an approximation of sub grid cell topographic variability. Our boundary conditions also include for the first time modelled estimates of Eocene aerosol distributions and tidal dissipation, both consistent with our palaeotopography and palaeobathymetry. The resolution of our data sets is unprecedented and will facilitate high resolution climate simulations. In light of the inherent uncertainties involved in reconstructing global boundary conditions for past time periods these data sets should be considered as one interpretation of the available data and users are encouraged to modify them according to their needs and interpretations. This paper marks the beginning of a process for reconstructing a set of accurate, open-access Eocene boundary conditions for use in climate models.

1 Introduction

Growth of the palaeoclimate modelling community has led to multiple independent efforts in modelling Eocene climate (Lunt et al., 2012). The growth in research groups modelling Eocene climate as well as the challenges faced by the community in capturing pertinent aspects of this period (Huber, 2012) make it desirable to distribute the boundary condition data sets used in published research. This serves two purposes: (1) that effort is not needlessly duplicated between research groups. The construction of boundary condition data sets for global climate models takes considerable effort and expertise. Thus, unless scientific disagreement exists, the process need only be conducted once; (2) that inter-model differences result only from variations in internal model assumptions and computational infrastructure. By holding boundary conditions fixed this enables a greater level of scientific understanding of the reasons for differences and commonalities between different groups' efforts. This was the impetus for the Paleoclimate Modelling Intercomparison Project (Braconnot et al., 2012), which assesses inter-model variation in Quaternary climate simulations and for which a consistent set of boundary conditions are openly available. Initiatives such as this have successfully fostered collaborations between research groups and provide a baseline for those wishing to conduct Quaternary climate simulations.

An ensemble of opportunity assembled in an ad hoc fashion – designated the Eocene Modelling Intercomparison Project (EoMIP) – has already been conducted using climate simulations described in studies published over the past several years (Lunt et al., 2012). Consequently, each model in this intercomparison differed at least partially with respect to their prescribed boundary condition forcing. In the spirit of encouraging data consistency within the Eocene climate modelling community we herein document a set of openly available and self-consistent climate model boundary conditions for the early Eocene (~ 55 Ma). While their intended application is in climate modelling, the broadening domain of geoscientific models may see them applied in a variety of numerical frameworks (e.g. Sect. 4). Specifically, this paper describes a newly updated Eocene topography, a necessary boundary condition for reconstructing past climates and one with a long history of inquiry (Donn and Shaw, 1977; Barron et al., 1981). An accompanying data set of sub grid cell topographic variability is also provided. We include a reconstructed Eocene bathymetry, which captures an unprecedented level of detail needed to meet the growing need for reconstructing regional Eocene oceanography (e.g. Hollis et al., 2012). The first estimate of Eocene tidal dissipation (Green and Huber, 2013) is also made available, complementing this recent addition to global climate models' suite of inputs and which may have particular relevance to Eocene climate (Lyle, 1997). Eocene vegetation simulated by an offline dynamic vegetation model is also discussed and provided. Simulated Eocene aerosol distributions are provided – again taking advantage of this recent addition to atmospheric models' prognostic capabilities – to account for the direct effects of Eocene dust, sea salt, sulfate, and organic and black carbon. Finally, river runoff directions are provided based on the gradient of Eocene topography. All of our data sets, with the exception of aerosol distributions, are made available at $1^\circ \times 1^\circ$ to facilitate high resolution global and regional simulations.

Previous efforts have been made to assemble self-consistent Eocene boundary conditions (Sewall et al., 2000; Bice et al., 1998) and provide motivation for our work here. While our boundary conditions incorporate more recent data and methodologies than most of those used previously, there are many aspects of Eocene tectonics and climate that remain uncertain or controversial. Thus in many regions our boundary conditions merely reflect one interpretation of the available data and may conflict with alternate interpretations (e.g. elevation of the North American Cordillera). Our aim here is not to propose a "correct" set of Eocene boundary conditions but to provide boundary conditions that can enable broader participation by the Eocene climate modelling community as well as greater transparency and reproducibility among groups. Researchers are encouraged to change these data sets based on their own data and interpretations.

2 Topography

2.1 Background and base data set

The palaeogeographic maps first used in climate modelling (Barron, 1980; Donn and Shaw, 1977) were semi-global in extent and were derived in large by Vinogradov (1967) and Phillips and Forsyth (1972). However, the first global Eocene palaeogeographic map applied to a climate model (Barron, 1985) was based on the work of Fred Ziegler and his colleagues at the University of Chicago, who had reconstructed a suite of Mesozoic to Cenozoic palaeotopographies (Ziegler et al., 1982). These palaeotopographies were built upon and succeeded by Christopher Scotese in the Paleomap Project (Scotese and Golonka, 1992), which was adopted by contemporary modelling efforts (Sloan and Rea, 1996; Sloan, 1994). Almost a decade later, Sewall et al. (2000) published a new global Eocene topography incorporating the latest regional tectonic data (Fig. 1a). For over a decade this data set has remained, without update, a highly utilized topography for Eocene climate modelling (Huber and Caballero, 2011; Winguth et al., 2009; Huber et al., 2003; Shellito et al., 2009; DeConto et al., 2012), and thus a data set incorporating more recent scholarship is overdue.

For both our Eocene topography and bathymetry we utilize base data sets that have been previously created. Here we adapt the early Eocene palaeotopographic map from Markwick (2007) (Fig. 1b). This map comes from a suite of Cretaceous to modern palaeotopographies which – similar to the Paleomap Project (Scotese and Golonka, 1992) – has its origins in the Paleogeographic Atlas Project at the University of Chicago (Ziegler et al., 1982). These maps have been augmented with more recent faunal, floral and lithological data and use a more recent rotation model (Rowley, 1995, unpublished). The primary method used to derive this Eocene topography is based on that described by Ziegler et al. (1985) and further documented by Markwick (2007), in which contour intervals of 1000 m or less are estimated by comparing past tectonic regimes to their present day analogues. Subsequent to this, adjustments to the palaeo-shoreline are made based on known Eocene biogeography (see Fig. 39 Markwick, 2007, for a map of known records). Thus, the palaeotopographic map of Markwick (2007) consists of a potential range of elevations for each grid cell, instead of an explicit value. A significant benefit of this method over others (e.g. Sewall et al., 2000) is obviation of the need for explicit palaeo-elevation estimates – which are scarce for most time periods and regions – while providing an approximate yet quantitative description of topography over a wide area of the Earth. The obvious limitation, however, is the lack of precision and topographic detail away from contour lines, which becomes significant in continental interiors where large anomalous plateaus appear (Fig. 1b).

Climate models require explicit and globally gridded elevation data so a conversion from the vector-based

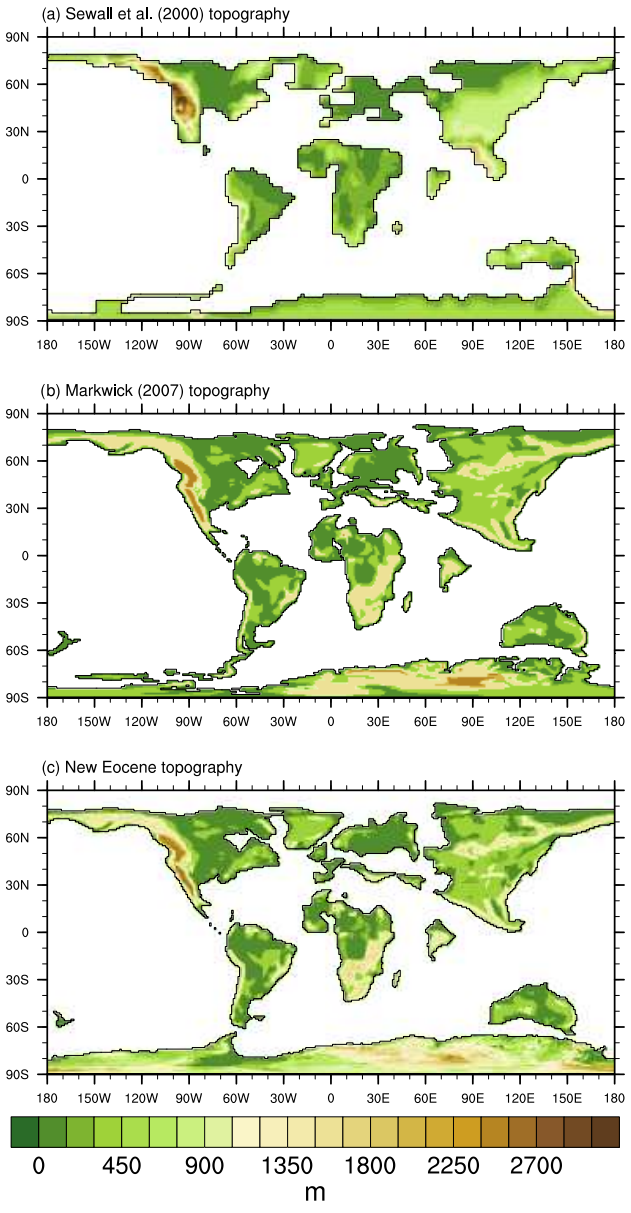

Figure 1. Eocene topography from **(a)** Sewall et al. (2000), **(b)** Markwick (2007) and **(c)** our revised early Eocene topography.

Geographic Information Systems approach underlying the topography of Markwick (2007) to a discrete digital elevation model was necessary. More importantly, detail in regions bounded by contour intervals was needed for which we applied a tension spline using the contour lines and sea level as tie points. This creates continuous discrete elevations at all locations. In order to provide plausible peak elevations and gradients along known mountain ranges (e.g. the North American and Andean Cordilleras) artificial tie points were added by inserting mountain spines in these areas. The process of interpolation was performed using the cssgrid function (Cubic Spline Sphere Gridder) from the National Center for Atmospheric Research (NCAR) Command Language (UCAR/NCAR/CISL/VETS, 2013) and a constant tension factor of 10, which provides a more linear interpolation between tie points as opposed to a pure cubic spline. This latter choice affects the roughness of the areas we interpolate between contour intervals.

2.2 Topographic revisions

Adjustments were made to conform the topography of Markwick (2007) to more recent or broadly accepted regional palaeogeographic reconstructions. For Antarctica we adopt the ANTscape "maximum" topographic reconstruction (Wilson et al., 2012) which incorporates, among other improvements, a more elevated West Antarctic bedrock than previous reconstructions have recognised (see Fig. 1). This ANTscape reconstruction is specifically for the Eocene–Oligocene boundary (∼ 34 Ma). However, it is significantly closer to the early Eocene than isostatically relaxed modern day bedrock (DeConto and Pollard, 2003; Pollard and DeConto, 2005). Our choice of the maximum reconstruction by Wilson et al. (2012) is also justified by the fact that the crust in the early Eocene was younger than at 34 Ma and that the interpolation required to adapt our topography to a given climate model inherently smooths high and complex relief. The resolution and scholarship of this reconstruction is also unprecedented, and given that no substantial continental ice existed between the early Eocene and Eocene–Oligocene transition (Cramer et al., 2011), uncertainty in the application of this data set only arises from regional tectonics and not emplacement of thick ice sheets. Future ANTscape reconstructions will include the early Eocene and may form a part of revisions to the global topography presented here (http://www.antscape.org/).

While our data set provides global coverage of land elevation there are several regions which suffer from large topographic uncertainty and which we highlight here. The proto-Himalayas along the southern margin of Eurasia is one such area. Prior to India's collision with Eurasia, between 55 and 45 Ma, geological evidence suggests Eurasia's southern margin may have been up to 4 km high (Molnar et al., 2010, and references therein). However, recent thermochronologic and cosmogenic nuclide data indicate relatively low relief persisted prior to collision (Hetzel et al., 2011). We choose to leave our data set as provided by Markwick (2007), with a peak elevation of 1500 m, which represents an intermediate solution to these competing uplift histories. This is a region where researchers with new data or interpretations may wish to make changes.

The uplift history of North American Cordillera is also subject to debate. Numerous palaeoaltimetry measurements based on oxygen isotope geochemistry suggest that western North America was relatively high, on the order of 3–4 km, since the early Cenozoic (e.g. Mix et al., 2011). However, palaeobotanical evidence suggests elevations were closer to

2 km (Wolfe et al., 1998) and it is known that atmospheric dynamics upwind of mountain ranges can significantly bias oxygen isotope records toward higher estimates of elevation (Galewsky, 2009). Thus we choose to constrain the maximum elevation of this region to the lower end of estimates, approximately 2500 m (Fig. 1c).

Despite the uncertainties in our reconstructed topography, there are several substantial improvements over the reconstruction of Sewall et al. (2000). In addition to the changes discussed above, our topography incorporates a more realistic extent of the Mississippi Embayment, reducing its area in accordance with marine carbonate, coal and peat distributions (Sessa et al., 2012; Markwick, 2007) (Fig. 1). The ANTscape Antarctic topography is also substantially more accurate than that of Sewall et al. (2000), which had an erroneously small continental area. The width of the Drake Passage is also reduced in our reconstruction to be more in accordance with data which imply an extremely nascent – i.e. oceanographically closed – gateway in the early Eocene (Barker et al., 2007; Lawver et al., 2011; Livermore et al., 2007). Palaeogeographical updates are also applied to Australia (Langford et al., 2001) and Europe (Iakovleva et al., 2001; Golonka, 2011; Torsvik et al., 2002). Our final Eocene topography is shown in Fig. 1c.

2.3 Representation of sub grid cell topographic variability

Numerous details at the sub grid cell scale have important effects on resolvable processes in global atmospheric models and thus require parameterisation. An important detail is the variation of topography within each grid cell, which allows models to parameterise atmospheric gravity waves based on surface roughness. Global atmospheric circulation models are sensitive to the parameterised wave drag and to their waves. These waves are important for the atmosphere's momentum balance, jet stream strength and the vertical transport of tracers, such as H_2O. In modern simulations the variability of sub grid cell topography is represented by the standard deviation of elevations within each model grid cell. For example, the variation of topography in a $1^\circ \times 1^\circ$ model grid cell is calculated from the standard deviation of all elevations within the $1^\circ \times 1^\circ$ domain using a $1' \times 1'$ data set (e.g. ETOPO1; Amante and Eakin, 2009). However, for past time periods knowledge of surface elevation at such a high resolution is impossible. To overcome this lack of information and provide an estimate of the Eocene variability of sub grid cell topography we use an empirical relationship between modern elevation and the standard deviation of sub grid cell topography, derived from the ETOPO1 data set (Amante and Eakin, 2009). A script that performs this task on a given topographic data set is provided in the Supplement.

In Fig. 2 we illustrate this process on our $1^\circ \times 1^\circ$ Eocene topography. Firstly, the modern ETOPO1 topography is regridded from its native $1' \times 1'$ resolution to $1^\circ \times 1^\circ$ (Fig. 2a), then, within each $1^\circ \times 1^\circ$ grid cell the standard deviation of elevations in the original ETOPO1 data set are calculated (Fig. 2b). The Greenland and Antarctic ice sheets are replaced with the appropriate bedrock topography given the smoothness of ice compared to continental crust. Secondly, an array of 100 m bins are created from 0 to 5500 m – representing the range of modern elevations – and the area-weighted average of the standard deviations of the grid cells that fall within each bin (calculated in the previous step) are calculated, resulting in an array of 55 values (Fig. 2c). Lastly, given the clear monotonic relation between height and standard deviation between sea level and approximately 3000 m, and between 3000 and 5500 m, separate linear regressions are calculated for these intervals (Fig. 2c) to assign estimates of Eocene variability in sub grid cell topography to each grid cell (Fig. 2d). Given that the maximum elevation in our Eocene topography is less than 3000 m (Fig. 1c) only the first linear regression is applicable here.

Figure 2c shows a peak in standard deviations of approximately 800 m at elevations between 2500 and 3500 m. This corresponds to the "Andean-type" environments identified by Ziegler et al. (1985) such as the boundaries of the Tibetan Plateau and Andean Cordillera (Fig. 2b). This broad peak remains regardless of the resolution we upscale ETOPO1 to, though its magnitude and width decreases with increasing resolution. Combined with an adequately derived atmospheric lapse rate, this data set of sub grid cell scale topographic variability may be used to constrain uncertainty in simulated surface temperatures which result from differences in the palaeo-elevation of a proxy record's site and the elevation resolved in a given climate model (e.g. Huber and Caballero, 2011; Sewall et al., 2000; Sewall and Sloan, 2006).

3 Bathymetry

3.1 Background and base data set

The first bathymetric maps used for Eocene ocean modelling constituted bowl-like basins in which the oceanic crust was treated primarily as abyssal plain (Barron and Peterson, 1991). The choice of a relatively flat bathymetry, although dictated to some extent by model resolution and available geological data, was informed by the lack of large scale oceanic responses to bathymetric details (Barron and Peterson, 1990). However, this result was misleading due to the lack of treatment of crucial oceanic processes in models of that generation (e.g. see Sect. 4). The most recent Eocene bathymetric data sets included the locations of mid-ocean ridges and shelf slope hypsometry (Bice et al., 1998; Huber et al., 2003). However, given that the highest level of detail in these data sets consist of only six depth classes and $\sim 3^\circ \times 1.5^\circ$ horizontal resolution, substantial gains are to be

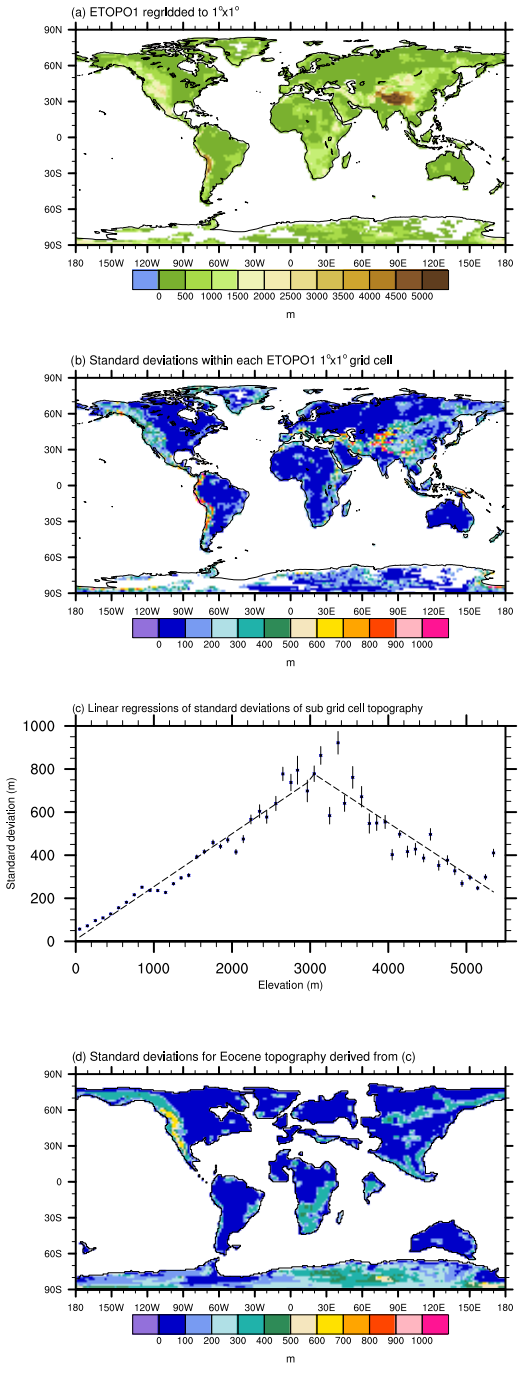

Figure 2. Estimating the standard deviation of sub grid cell elevations for the Eocene. **(a)** ETOPO1 topography downscaled from its native $1' \times 1'$ resolution to $1° \times 1°$. **(b)** Standard deviation of $1' \times 1'$ elevations inside each $1° \times 1°$ grid cell. **(c)** Standard deviations from **(b)** area-weight averaged into 100 m bins and plotted against corresponding elevation. Standard error for each bin is plotted. Dotted lines represent linear regressions between sea level and 3000, and 3000 and 5500 m. **(d)** Linear regressions from **(c)** applied to Eocene topography (Fig. 1c). See text for details.

made by employing new methodologies and higher resolution base data sets to reconstruct Eocene bathymetry.

The base data set for our bathymetry is formed from the global 55 Ma bathymetry of Müller et al. (2008b), which is part of a suite of palaeobathymetric maps reconstructed from 140 Ma to the present. Like previous efforts the foundation of this bathymetry is the application of an age–depth relationship to reconstructed seafloor spreading isochrons. As lithospheric crust ages and cools on its path away from the mid-ocean ridge, thinning occurs (Fig. 3a and b). In constructing our Eocene bathymetry the age–depth relationship derived by Stein and Stein (1992) was applied to reconstructed 55 Ma seafloor ages:

$$\text{if } t < 20 \text{ Ma; } d(t) = 2600 + 365t^{1/2},$$
$$\text{if } t \geq 20 \text{ Ma; } d(t) = 5651 - 2473\exp(-0.0278t),$$

where d is the basement depth in metres and t is time in Myr. Several age–depth relationships have been previously tested to determine the best match to modern bathymetry, with Stein and Stein (1992) showing the least bias (Müller et al., 2008b). To accommodate regions where Eocene crust is not available at present (due to the subsequent subduction of oceanic crust) symmetric mid-ocean ridge spreading was assumed and seafloor spreading isochrons from the conjugate plate applied. In regions where no data were available from the conjugate plate, interpolation was applied between available isochrons and the adjacent plate margin (Müller et al., 2008a, b).

On tectonic timescales (Myr) the development of large igneous provinces (LIPs) can have significant impacts on global sea level (Müller et al., 2008b) and ocean circulation (Lawver et al., 2011), thus LIPs form an important component of our Eocene bathymetry. These bathymetric features are reconstructed by applying modern LIP outlines and estimating palaeo-LIP height following Schubert and Sandwell (1989). Additionally, given that certain regions of the modern ocean are covered by up to several kilometres of sediment (Whittaker et al., 2013) reconstructed sediment thicknesses also represent an important component of our reconstructed palaeobathymetry. Based on an empirical relationship with age and latitude (polar latitudes generally having larger river runoff and tropical latitudes subject to high marine productivity), an age–latitude relationship was applied (Müller et al., 2008b, Supplement) to reconstruct Eocene sediment thickness (Fig. 3c).

3.2 Bathymetric revisions

While the methodology adopted from Müller et al. (2008b) represents a substantial improvement over previous bathymetric maps, it is by design a generic process used to reconstruct bathymetry over the past 140 Myr. Therefore discrepancies exist in some regions where palaeoceanographic data have been recovered. Particularly, the depths of certain LIPs may be verified against known depth habitats of

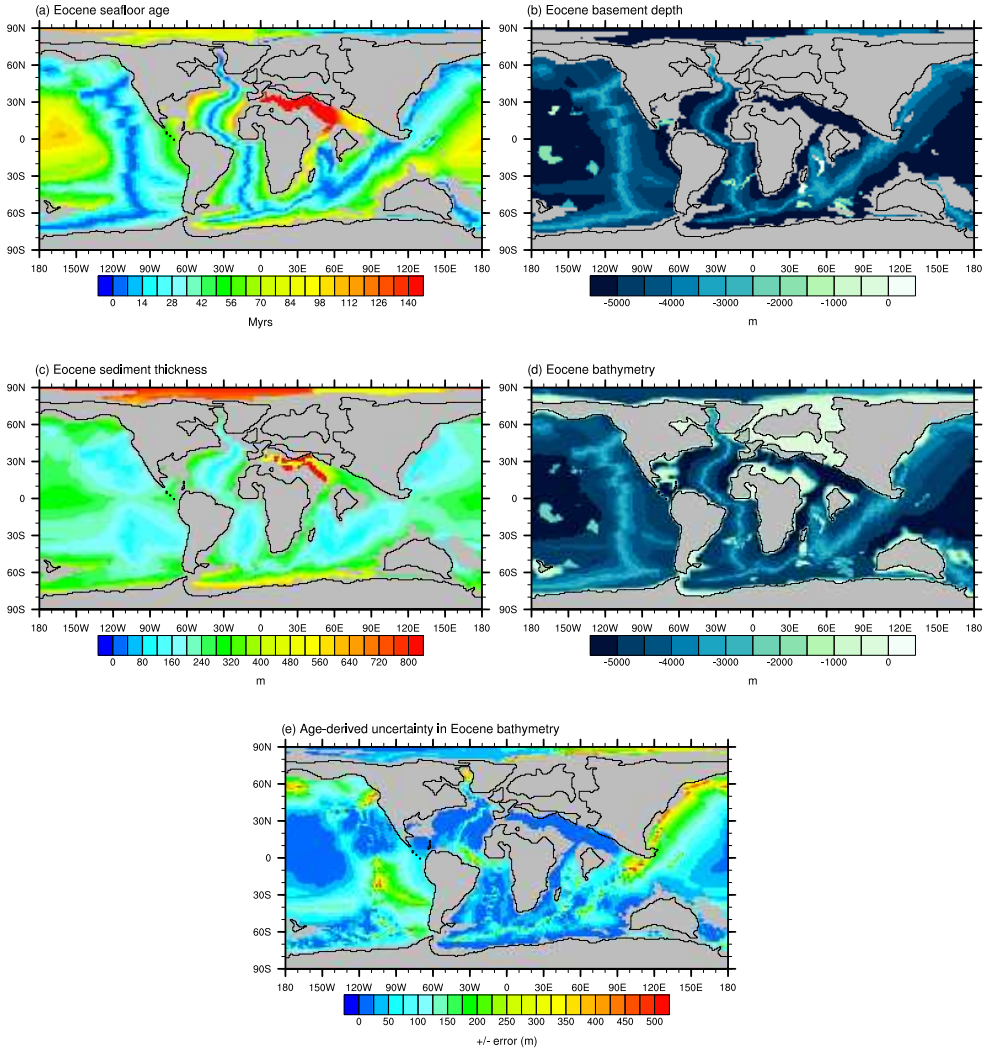

Figure 3. 55 Ma **(a)** seafloor age, **(b)** basement depth, **(c)** sediment thickness, **(d)** final bathymetry and **(e)** the error margin in our bathymetry based on age uncertainty (values represent the range of uncertainty above and below the bathymetry shown in **(d)**. Black outlines indicate palaeo-shoreline.

foraminifera recovered from deep-sea cores. Such a verification was carried out here using Deep Sea Drilling Project and Ocean Drilling Project records. Based on these records the depth of the Madagascar Ridge (Schlich, 1974), Mascarene Ridge (Backman et al., 1988; Fisher et al., 1974; Vincent et al., 1974), Shatsky Rise, Ontong Java Plateau (Barrera et al., 1993), Kerguelen Plateau (Mackensen and Berggren, 1992), Walvis Ridge (Zachos et al., 2005; Fuetterer, 1984) and the Rio Grande Rise (Perch-Nielsen et al., 1977) were adjusted.

Reconstructing the tectonic history of ocean gateways is critical in explaining past ocean circulation (Scher and Martin, 2006; Hill et al., 2013), faunal migration patterns (Dalziel et al., 2013a) and potentially global climate change (Barker and Thomas, 2004). The Drake Passage and Tasman gateway are of particular significance given that their opening was a requirement for development of the Antarctic Circumpolar Current, the largest ocean current in the world ($\sim$ 130 Sv) and the only circum global one (Barker and Thomas, 2004). Unfortunately, the Drake Passage suffers from poor age constraints due to the tectonically complex Scotia arc region and estimates of its opening range from the middle Eocene to late Miocene (Dalziel et al., 2013b; Scher and Martin, 2006). As our bathymetry represents the early Eocene we prescribe an oceanographically closed Drake Passage, constraining its depth to less than 100 m. Multiple palaeoceanographic and tectonic records indicate that the Tasman gateway did not open to deep flow until the late Eocene (Stickley et al., 2004), although when a shallow opening appeared is debatable. Our reconstruction of tectonic plate positions as well as the location of Tasmania suggests that a shallow epicontinental sea may have existed and thus we prescribe a depth of 30 m or less in the Tasman gateway. Finally, no data are available for

the bathymetry of inland seas or continental shelves in our base data sets and thus we assume a maximum depth of 50 m for inland seas and use a Poisson equation solver to interpolate intermediate values for both areas. Figure 3d shows our final Eocene bathymetry. The uncertainty in this bathymetry is shown in Fig. 3e as a function of age uncertainty, with largest values in the southeast and northwest Pacific Ocean (Fig. 3a).

3.3 Consistent plate rotations

The plate rotation model used to construct our palaeobathymetry differs from that used for our palaeo-topography (Sect. 2). To maintain a consistent reference frame between the two data sets we re-rotate our Eocene topography using the plate rotation model of Müller et al. (2008b). This was achieved by changing the reference plate (Africa) location from that determined by Ziegler to that determined by Müller et al. (2008b), resulting in a relative shift of the other continents. Refinements to the location of some continental blocks were made to improve the match between the locations of continental crust in both data sets. These steps were largely achieved using the open source software packages GPlates (http://www.gplates.org/), for digitizing polygons, and Generic Mapping Tools (http://gmt.soest.hawaii.edu/) for manual corrections. Deep integration of plate rotation software with open access palaeontology databases has the potential to streamline future palaeogeographic reconstructions (e.g. Wright et al., 2013). The final merged Eocene topography and bathymetry is shown in Fig. 4 alongside ETOPO1.

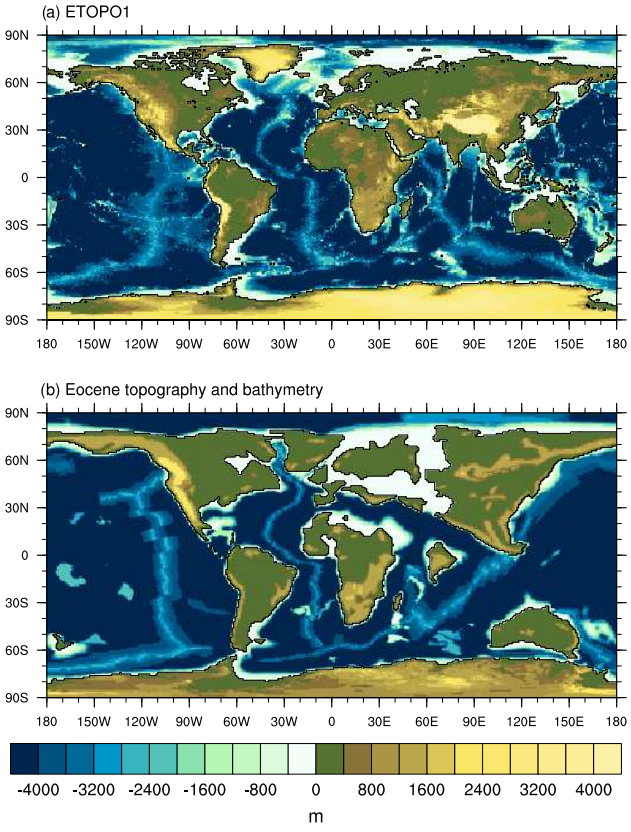

Figure 4. (a) ETOPO1 topography and bathymetry, **(b)** new Eocene topography and bathymetry. Both at $1^\circ \times 1^\circ$ resolution.

4 Tidal dissipation

The importance of tidal dissipation in the ocean's general circulation stems from the fact that diapycnal (i.e. vertical) mixing is greatly affected by the tide's interaction with bathymetry. Large increases in diapycnal mixing are observed above regions of rough topography (e.g. Polzin et al., 1997) and are primarily a result of breaking tidally induced internal waves (Garrett and Kunze, 2007; Jayne et al., 2004). Tidal models have been used to predict the amount of tidal energy dissipated in the oceans and to better constrain vertical mixing profiles incorporated in ocean general circulation models (e.g. Simmons et al., 2004). Such experiments have demonstrated that tidal energy considerations significantly reduce the discrepancy between simulated and observed modern ocean heat transport (Simmons et al., 2004) and provides motivation for explicitly including tidal dissipation in past climate simulations (e.g. Green and Huber, 2013; Egbert et al., 2004).

New atmosphere–ocean general circulation models are beginning to incorporate tidal dissipation (e.g. the Community Earth System Model; CESM; Gent et al., 2011). Green and Huber (2013) applied a tidal model using the bathymetry described in Sect. 3 and showed that, while total Eocene tidal dissipation was weaker than present, a larger amount of tidal energy was dissipated in the deep ocean, especially in the deep Pacific. The vertical diffusivities associated with these results are significantly larger than present, supporting arguments that enhanced vertical mixing in the Eocene oceans helps to explain the low equator to pole temperature gradient inferred from geological records (e.g. Lyle, 1997), but that have hitherto been difficult to reproduce in models (Lunt et al., 2012).

We distribute the data set from Green and Huber (2013) here as a map of energy dissipated per unit area (Fig. 5). Models such as the National Center for Atmospheric Research CESM can utilize this data set to drive their tidal mixing schemes. While this work represents a coarse first attempt at deriving Eocene tidal dissipation, to our knowledge no similar effort has been made and thus this data set provides a baseline for groups who do not have access to the tools required for deriving this boundary condition. However, given the infancy of this application to deep time palaeoclimate it is likely that such a data set will be improved upon quickly.

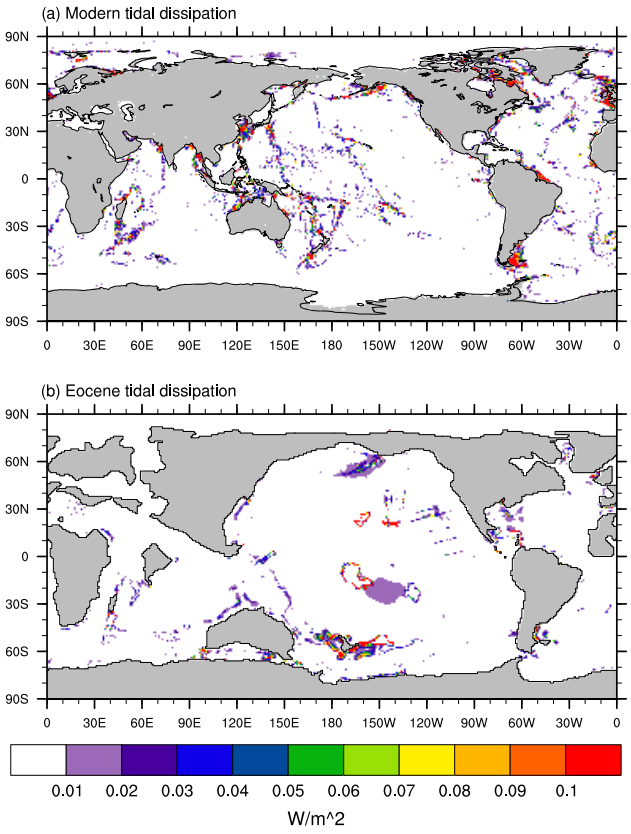

Figure 5. (a) Modern and **(b)** Eocene simulated tidal dissipation (Green and Huber, 2013).

5 Vegetation

Climate models have long shown substantial global and regional climatic responses to vegetation change (Otto-Bliesner and Upchurch, 1997; Dutton and Barron, 1997), though newer models indicate a weaker sensitivity (Henrot et al., 2010; Micheels et al., 2007). A series of Tertiary vegetation maps based on palaeofloral records (Wolfe, 1985) formed the foundation of many early palaeoclimate simulations that explicitly included a palaeovegetation boundary condition (e.g. Sloan and Rea, 1996; Dutton and Barron, 1997). Subsequently, Sewall et al. (2000) developed a new Eocene vegetation distribution taking into account more recent data and the effects of a low equator-to-pole temperature gradient. Like their Eocene topography, the vegetation reconstruction of Sewall et al. (2000) has remained highly utilized by the Eocene climate modelling community (e.g. Huber et al., 2003; Liu et al., 2009; Roberts et al., 2009; Huber and Caballero, 2011; Shellito et al., 2003).

We choose to reconstruct early Eocene vegetation using the offline dynamic vegetation model BIOME4 (Kaplan et al., 2003). For input into BIOME4 we use temperature, precipitation and cloud cover from a CESM simulation forced with the Eocene topography and bathymetry described in Sects. 2 and 3, respectively, and an atmospheric CO_2 concentration of 2240 ppmv, a concentration which has been found to approximately reproduce Eocene temperatures (Huber and Caballero, 2011). This CESM simulation was integrated for 250 years and initialized with output from a previous CESM simulation that was integrated for over 3000 years (this latter simulation was forced with the boundary conditions of Sewall et al. (2000) for topography and vegetation, and Huber et al. (2003) for bathymetry, mixed-layer ocean simulations of which are described by Goldner et al. (2013)). The BIOME4 was forced with a CO_2 concentration of 1120 ppmv since higher concentrations resulted in large scale reductions in tropical forest. While this is not consistent with the CO_2 forcing of the driving climatology we are here only interested in deriving a vegetation distribution that is feasibly "Eocene" in character. Figure 6a and b shows the simulated pre-industrial and Eocene distributions of biomes, respectively. For ease of comparison we show these biome maps simplified from the 27 biomes simulated by BIOME4 to 10 mega biomes after Harrison and Prentice (2003). Our BIOME4 simulated vegetation compares well with vegetation inferred from Palaeocene and Eocene palynoflora (Utescher and Mosbrugger, 2007; Morley, 2007) and are consistent with geological indicators of climate (Crowley, 2012). One apparent bias is an abundance of relatively dry vegetation in northern South America in BIOME4 (Morley, 2007). However, there remains a distinct lack of records for validation from large regions of South Africa and Siberia. We also note that "grass" did not exist at the biome level in the Eocene (Strömberg, 2011), and thus the "Grassland and dry shrubland" biome presented in Fig. 6 should be interpreted as shrubland only. Our vegetation reconstruction reflects our simulated Eocene climate and is therefore less zonal than previous reconstructions (Sewall et al., 2000) and is consistent with our Eocene topography.

The utilisation of a single climate simulation to drive BIOME4 inherently results in a vegetation distribution that encompasses the biases of our climate model. While utilisation of ensemble climate model data (Lunt et al., 2012) would attenuate individual model biases such data sets would deteriorate the representation of our new topography in the simulated vegetation. For example, many of the models evaluated in EoMIP were forced with the topography of Sewall et al. (2000) in which certain continents were several degrees of latitude or longitude offset from our new topography. Furthermore, most of these simulations were run at a substantially lower resolution than done here. Thus, utilising such data sets would result in mountainous vegetation – for example over the North American cordillera – not completely corresponding to the location of mountain ranges in our topography. Such an issue may be improved over time as more simulations are conducted with the topographic boundary condition presented here.

Due to the significant differences between modern and Eocene topography (Fig. 4), the anomaly method typically

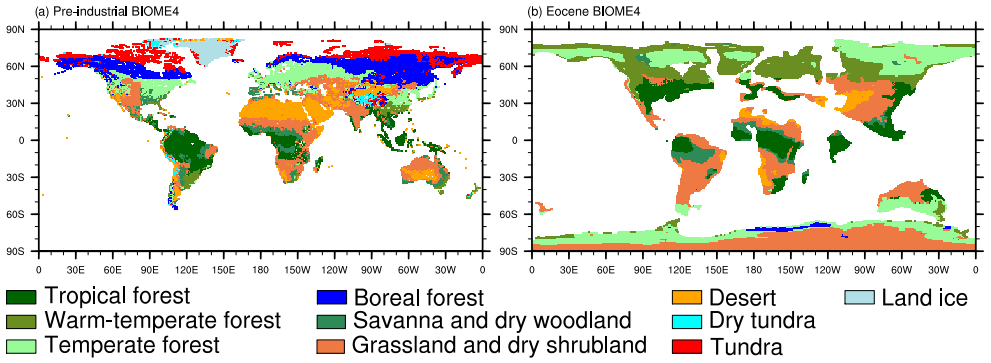

Figure 6. (a) Pre-industrial and **(b)** Eocene vegetation simulated by BIOME4. The 27 biomes simulated by BIOME4 have been consolidated into 10 mega biomes following Harrison and Prentice (2003).

used for specifying input into the BIOME4 (Kaplan et al., 2003) was not possible and thus first order biases in our control CESM simulation are not taken into consideration. However, given that the CESM simulates modern land and sea-surface temperatures broadly consistent with observations (Gent et al., 2011) and that the biases in the modern CESM climate are small in comparison with the simulated change in climate for the Eocene (Huber and Caballero, 2011) we do not believe this to be a significant issue. Furthermore, while asynchronous coupling between our climate and vegetation models precludes the ability of the simulated vegetation to affect climate – as compared to synchronous coupling efforts (e.g. Shellito and Sloan, 2006a, b) – it benefits our results by not erroneously amplifying biases in our climate model (e.g. Wohlfahrt et al., 2008).

6 Aerosols

Aerosols in Eocene climate simulations have previously been prescribed at pre-industrial levels or set to arbitrarily determined, globally uniform values. Aerosols constitute one of the largest uncertainties in radiative forcing under future anthropogenic greenhouse warming (Stocker et al., 2013) and may be important in resolving some long standing palaeoclimate conundrums (Kump and Pollard, 2008). Insufficient proxies from the pre-Quaternary prevent the reconstruction of this boundary condition from geological records. However, the advent of aerosol prognostic capabilities in atmospheric models allows the palaeo-distribution of various aerosol species to be simulated (Heavens et al., 2012). Here we again employ the NCAR CESM in a configuration that utilizes the newly implemented Bulk Aerosol Model, which is a component of the Community Atmosphere Model 4 (Neale et al., 2010). In this configuration the model explicitly simulates the monthly horizontal and vertical distribution of dust, sea salt, sulfate, and organic and black carbon aerosols consistent with our Eocene topography (Fig. 7). The Bulk Aerosol Model makes simplistic assumptions regarding the size distribution of aerosol species, compared to the more complicated Modal Aerosol Models. A detailed description of the steps involved in simulating the palaeo-distribution of aerosols is provided by Heavens et al. (2012). Here we branch the same CESM simulation described in Sect. 5 while also enabling the Bulk Aerosol Model.

Various aerosol species require the prescription of emission sources in the Bulk Aerosol Model and this is done in accordance with Heavens et al. (2012). One exception is that we do not specify any volcanic sources of SO_2 or SO_4, given their small radiative effects and the uncertainty in the distribution of Eocene volcanoes. Another largely unconstrained yet climatically relevant emission source in the Bulk Aerosol Model is that of dust. In the Bulk Aerosol Model dust is emitted solely from the desert plant functional type which in turn is determined from the prescribed vegetation data set. It is generally understood that cooler climates promote more dust-laden atmospheres – due to increases in desertification, reduced soil moisture and stronger winds (Bar-Or et al., 2008). However, the degree to which global Eocene dust concentrations differed from typical glacial–interglacial variability is uncertain, though regional evidence exists for substantially weak dust fluxes in the early Cenozoic (Janecek and Rea, 1983). Here we have assumed that global Eocene dust loading was approximately three quarters that of the pre-industrial era. The sources of dust in our data set (i.e. deserts) were manually distributed based loosely on the distribution of early Eocene evaporites (Crowley, 2012), which itself follows the expected distribution of subtropical high pressure regions. Our chosen concentrations provide an Eocene dust loading intermediate to simulations which prescribe pre-industrial values (e.g. Heinemann et al., 2009; Lunt et al., 2010; Winguth et al., 2009) and those which eliminate the radiative effects of aerosols altogether (Huber and Caballero, 2011). The significant improvement in the approach taken here is that the distribution of aerosols is consistent with our Eocene topography, providing a realistic regional representation of their radiative forcing.

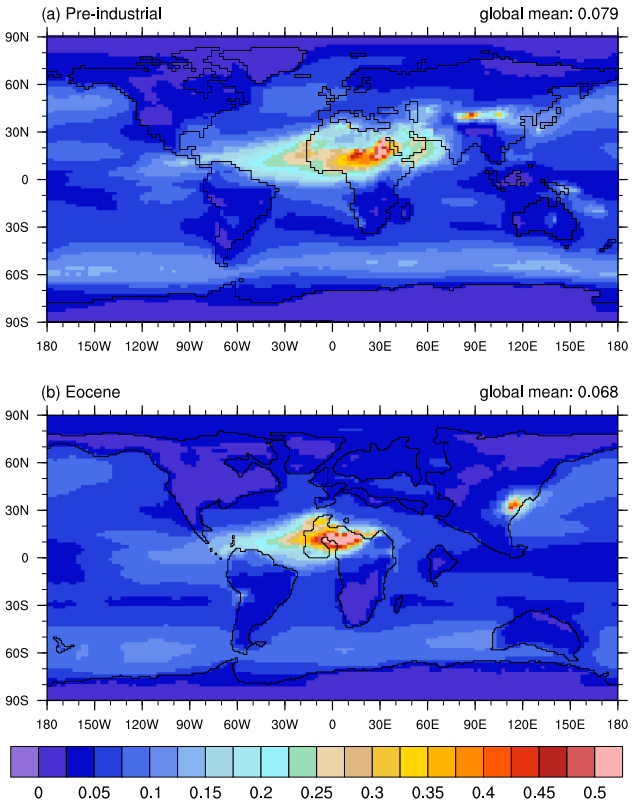

Figure 7. (a) Pre-industrial and **(b)** Eocene aerosol optical depth (unitless) simulated by the Community Atmosphere Model 4.

It is important to stress the large uncertainty in aerosol loading and distribution during past climates and that our simulated concentrations are likely highly model dependant. Furthermore, the aerosol data sets provided here are only adequate for models that do not include the indirect effects of aerosols. Models that include such effects may exhibit significant sensitivity to even slight changes in aerosol distribution and loading and we are not confident that the use of the data sets presented here, given the uncertainties involved, would be scientifically sound.

Finally, we note that the ability to prognose aerosol distributions in long climate simulations (available in the latest atmospheric models, though at significant computational cost) will obviate the need for prescribed aerosol concentrations while also accounting for their indirect effects. Such models will see the emission sources of various aerosol species (e.g. deserts, volcanoes, regions of high marine productivity) become an additional palaeoclimate model boundary condition.

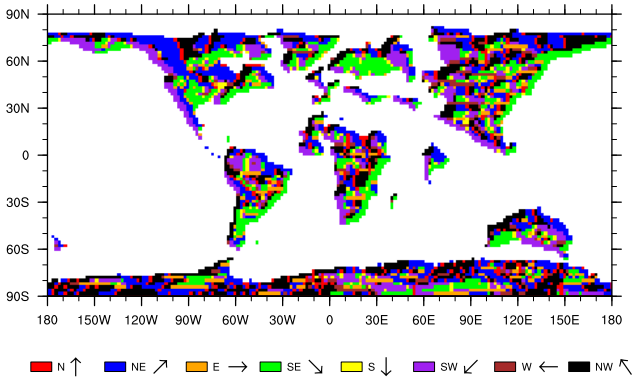

Figure 8. Eocene river runoff directions. Directions indicated by colour.

7 River transport

River runoff in current generation climate models is important primarily for the redistribution of fresh water to the oceans and can have significant implications for deep water formation (e.g. Bice et al., 1997). Here we use the gradient of our Eocene topography to represent river runoff direction (Fig. 8). This data set was created using scripts made available by the National Center for Atmospheric Research (Rosenbloom et al., 2011). Regions where vectors do not reach the ocean (i.e. internal basins) were manually corrected. Topographic gradient has been used to constrain river directions in the overwhelming majority of palaeoclimate simulations to date. However, it is a crude method which we show here simply for completeness. Furthermore, the data set provided (Fig. 7) is only illustrative as the regridding of our topography (Fig. 1) to a given climate model's resolution will require re-calculation of these river directions to account for changes in gradient. A more morphologically constrained river direction data set (e.g. Markwick and Valdes, 2004) should be integrated into future revisions of our Eocene boundary conditions.

8 Discussion and future work

We describe an openly available and comprehensive set of early Eocene climate model boundary conditions including topography, bathymetry, tidal dissipation, vegetation, aerosols and river transport. The resolution of most of these data sets is unprecedented and alleviates the undesirable step of upscaling lower resolution data sets to that of current generation climate models. This should lead to improvements in model–data comparison in regions of strong relief and facilitate high resolution global and regional climate simulations.

An important distinction between our tidal, vegetation, aerosol data sets and our topography and bathymetry data sets is that the former are model derived and thus not directly based on measured physical quantities. The use of modelling

frameworks for our tidal and aerosol boundary conditions is necessitated by the absence of any quantitative Eocene data. Our use of a model to derive Eocene vegetation was predicated on the model's ability to capture what is known about Eocene vegetation from palaeobotanical records (model validation). As this is the case (see Sect. 5) we can have an at least (or perhaps at best) satisfactory level of confidence that the model is not predicting unrealistic vegetation in regions where data are scarce. This eliminates the need for researchers to subjectively estimate vegetation for large swathes of land, though of course is directly affected by the climate biases of our driving climatology.

Despite the substantial improvements introduced in these boundary conditions, uncertainties in the data remain. These are most pertinent in the palaeo-elevation of the North American Cordillera and proto-Himalayas, the geometry of the Drake Passage and Tasman Gateway, our modelled tidal dissipation and aerosol distributions and lastly our rudimentary representation of river runoff. These data- and model-based uncertainties provide a natural focus for future research in developing new methods of inquiry (or eliminating old ones) and in focusing efforts on data collection. Reconciling tectonic models and palaeo-elevation proxies will be crucial for reducing palaeotopographic uncertainty in revised versions of these boundary conditions. On the other hand, advances in modelling may substantially improve the reconstruction of tidal dissipation and aerosol distributions, though quantitative validation of either of these in the Eocene is next to impossible.

Finally, as important as the input into any model representing a real-world system is, an at least equal importance should be placed on the data against which such models are validated. Fortunately, recent compilations of terrestrial and marine data have already been conducted by Huber and Caballero (2011) and Lunt et al. (2012), respectively. We stress that the maintenance and public availability of such data sets provides the necessary yardstick against which to compare all models. Users are also able to rotate newly collected data to their 55 Ma position in the same reference frame used here via the open source software package GPlates (http://www.gplates.org/), thus ensuring that consistency in georeferencing is maintained. A community effort to adopt consistent modelling methodologies and boundary conditions can accelerate growth in our understanding of Eocene climates and specifically help highlight the most pertinent shortcomings of the current generation of climate models in simulating extreme greenhouse warmth.

The Supplement related to this article is available online at doi:10.5194/gmd-7-2077-2014-supplement.

Acknowledgements. N. Herold, J. Buzan, A. Goldner and M. Huber are supported under *1049921-EAR: Collaborative Research: Improved Cenozoic paleoelevation estimates for the Sierra Nevada, California: Linking geodynamics with atmospheric dynamics*. M. Seton and R. D. Müller acknowledge support from Australian Research Council (ARC) grants DP0987713 and FL0992245, respectively. The tidal model simulations were funded by the Natural Environmental Research Council (grant NE/F014821/1) and the Climate Change Consortium for Wales (JAMG), and the National Science Foundation (grant 0927946-ATM to M. Huber). The NCAR Command Language (NCL) was used to create our figures. NCL and Generic Mapping Tools were used for the manipulation of data.

Edited by: D. Lunt

References

Amante, C. and Eakin, B. W.: ETOPO1 1 Arc-Minute Global Relief Model: Procedures, Data Sources and Analysis, NOAA Technical Memorandum, 2009.

Backman, J., Duncan, R. A., Peterson, L. C., Baker, P. A., Baxter, A. N., Boersma, A., Cullen, J. L., Droxler, A. W., Fisk, M. R., Greenough, J. D., Hargraves, R. B., Hempel, P., Hobart, M. A., Hurley, M. T., Johnson, D. A., Macdonald, A. H., Mikkelsen, N., Okada, H., Rio, D., Robinson, S. G., Schneider, D., Swart, P. K., Tatsumi, Y., Vandamme, D., Vilks, G., and Vincent, E.: Site 707, ODP Ocean Drilling Program, 1988.

Bar-Or, R., Erlick, C., and Gildor, H.: The role of dust in glacial–interglacial cycles, Quaternary Sci. Rev., 27, 201–208, doi:10.1016/j.quascirev.2007.10.015, 2008.

Barker, P. F. and Thomas, E.: Origin, signature and palaeoclimatic influence of the Antarctic Circumpolar Current, Earth-Sci. Rev., 66, 143–162, 2004.

Barker, P. F., Filippelli, G. M., Florindo, F., Martin, E. E., and Scher, H. D.: Onset and role of the Antarctic Circumpolar Current, Deep Sea Res. Pt. II, 54, 2388–2398, doi:10.1016/j.dsr2.2007.07.028, 2007.

Barrera, E. B., Lohmann, J., and Kyger, C.: Strontium isotope and benthic foraminifer stable isotope results from Oligocene sediments at Site 803, ODP Ocean Drilling Program, 1993.

Barron, E. J.: Paleogeography and Climate, 180 Million Years to the Present, University of MIAMI, 1980.

Barron, E. J.: Explanations of the Tertiary global cooling trend, Palaeogeogr. Palaeocl., 50, 45–61, 1985.

Barron, E. J. and Peterson, W. H.: Mid-Cretaceous ocean circulation: Results from model sensitivity studies, Paleoceanography, 5, 319–337, doi:10.1029/PA005i003p00319, 1990.

Barron, E. J. and Peterson, W. H.: The Cenozoic ocean circulation based on ocean General Circulation Model results, Palaeogeogr. Palaeocl., 83, 1–28, 1991.

Barron, E. J., Thompson, S. L., and Schneider, S. H.: An Ice-Free Cretaceous? Results from Climate Model Simulations, Science, 212, 501-508, doi:10.1126/science.212.4494.501, 1981.

Bice, K. L., Barron, E. J., and Peterson, W. H.: Continental runoff and early Cenozoic bottom-water sources, Geology, 25, 951–954, 1997.

Bice, K. L., Barron, E. J., and Peterson, W. H.: Reconstruction of realistic early Eocene paleobathymetry and ocean GCM sensi-

tivity to specified basin configuration, Oxford Monographs on Geology and Geophysics, 39, 227–247, 1998.

Braconnot, P., Harrison, S. P., Kageyama, M., Bartlein, P. J., Masson-Delmotte, V., Abe-Ouchi, A., Otto-Bliesner, B., and Zhao, Y.: Evaluation of climate models using palaeoclimatic data, Supplement, Nature Clim. Change, 2, 417–424, 2012.

Cramer, B. S., Miller, K. G., Barrett, P. J., and Wright, J. D.: Late Cretaceous–Neogene trends in deep ocean temperature and continental ice volume: Reconciling records of benthic foraminiferal geochemistry (δ^{18}O and Mg/Ca) with sea level history, J. Geophys. Res.-Oceans, 116, C12023, doi:10.1029/2011jc007255, 2011.

Crowley, C. W.: An atlas of Cenozoic climates, Masters of science in geology, The University of Texas, 2012.

Dalziel, I. W. D., Lawver, L. A., Norton, I. O., and Gahagan, L. M.: The Scotia Arc: Genesis, Evolution, Global Significance, Annu. Rev. Earth Pl. Sc., 41, 767–793, doi:10.1146/annurev-earth-050212-124155, 2013a.

Dalziel, I. W. D., Lawver, L. A., Pearce, J. A., Barker, P. F., Hastie, A. R., Barfod, D. N., Schenke, H.-W., and Davis, M. B.: A potential barrier to deep Antarctic circumpolar flow until the late Miocene?, Geology, 41, 947–950, doi:10.1130/g34352.1, 2013b.

DeConto, R. M. and Pollard, D.: Rapid Cenozoic glaciation of Antarctica induced by declining atmospheric CO_2, Nature, 421, 245–249, 2003.

DeConto, R. M., Galeotti, S., Pagani, M., Tracy, D., Schaefer, K., Zhang, T., Pollard, D., and Beerling, D. J.: Past extreme warming events linked to massive carbon release from thawing permafrost, Supplement, Nature, 484, 87–91, 2012.

Donn, W. L. and Shaw, D. M.: Model of climate evolution based on continental drift and polar wandering, Geol. Soc. Am. Bull., 88, 390–396, doi:10.1130/0016-7606(1977)88<390:mocebo>2.0.co;2, 1977.

Dutton, J. F. and Barron, E. J.: Miocene to present vegetation changes; a possible piece of the Cenozoic cooling puzzle, Geology, 25, 39–41, 1997.

Egbert, G. D., Ray, R. D., and Bills, B. G.: Numerical modeling of the global semidiurnal tide in the present day and in the last glacial maximum, J. Geophys. Res.-Oceans, 109, C03003, doi:10.1029/2003jc001973, 2004.

Fisher, R. L., Bunce, E. T., Cernock, P. J., Clegg, D. C., Cronan, D. S., Damiani, V. V., Dmitriev, L. V., Kinsman, D. J., Roth, P. H., Thiede, J., and Vincent, E.: Site 237, DSDP Deep Sea Drilling Project, 1974.

Fuetterer, D. K.: Bioturbation and trace fossils in deep sea sediments of the Walvis Ridge, southeastern Atlantic, Leg 74, DSDP Deep Sea Drilling Project; IPOD International Phase of Ocean Drilling, 1984.

Galewsky, J.: Orographic precipitation isotopic ratios in stratified atmospheric flows: Implications for paleoelevation studies, Geology, 37, 791–794, doi:10.1130/g30008a.1, 2009.

Garrett, C. and Kunze, E.: Internal Tide Generation in the Deep Ocean, Annu. Rev. Fluid Mech., 39, 57–87, doi:10.1146/annurev.fluid.39.050905.110227, 2007.

Gent, P. R., Danabasoglu, G., Donner, L. J., Holland, M. M., Hunke, E. C., Jayne, S. R., Lawrence, D. M., Neale, R. B., Rasch, P. J., Vertenstein, M., Worley, P. H., Yang, Z.-L., and Zhang, M.: The Community Climate System Model Version 4, J. Climate, 24, 4973–4991, doi:10.1175/2011jcli4083.1, 2011.

Goldner, A., Huber, M., and Caballero, R.: Does Antarctic glaciation cool the world?, Clim. Past, 9, 173–189, doi:10.5194/cp-9-173-2013, 2013.

Golonka, J.: Chapter 6 Phanerozoic palaeoenvironment and palaeolithofacies maps of the Arctic region, Geological Society, London, Memoirs, 35, 79–129, doi:10.1144/m35.6, 2011.

Green, J. A. M. and Huber, M.: Tidal dissipation in the early Eocene and implications for ocean mixing, Geophys. Res. Lett., 40, 2707–2713, doi:10.1002/grl.50510, 2013.

Harrison, S. P. and Prentice, C. I.: Climate and CO_2 controls on global vegetation distribution at the last glacial maximum: Analysis based on palaeovegetation data, biome modelling and palaeoclimate simulations, Global Change Biol., 9, 983–1004, 2003.

Heavens, N. G., Shields, C. A., and Mahowald, N. M.: A paleogeographic approach to aerosol prescription in simulations of deep time climate, Journal of Advances in Modeling Earth Systems, 4, M11002, doi:10.1029/2012ms000166, 2012.

Heinemann, M., Jungclaus, J. H., and Marotzke, J.: Warm Paleocene/Eocene climate as simulated in ECHAM5/MPI-OM, Clim. Past, 5, 785–802, doi:10.5194/cp-5-785-2009, 2009.

Henrot, A.-J., François, L., Favre, E., Butzin, M., Ouberdous, M., and Munhoven, G.: Effects of CO_2, continental distribution, topography and vegetation changes on the climate at the Middle Miocene: a model study, Clim. Past, 6, 675–694, doi:10.5194/cp-6-675-2010, 2010.

Hetzel, R., Dunkl, I., Haider, V., Strobl, M., von Eynatten, H., Ding, L., and Frei, D.: Peneplain formation in southern Tibet predates the India-Asia collision and plateau uplift, Geology, 39, 983–986, doi:10.1130/g32069.1, 2011.

Hill, D. J., Haywood, A. M., Valdes, P. J., Francis, J. E., Lunt, D. J., Wade, B. S., and Bowman, V. C.: Paleogeographic controls on the onset of the Antarctic circumpolar current, Geophys. Res. Lett., 40, 5199–5204, doi:10.1002/grl.50941, 2013.

Hollis, C. J., Taylor, K. W. R., Handley, L., Pancost, R. D., Huber, M., Creech, J. B., Hines, B. R., Crouch, E. M., Morgans, H. E. G., Crampton, J. S., Gibbs, S., Pearson, P. N., and Zachos, J. C.: Early Paleogene temperature history of the Southwest Pacific Ocean: Reconciling proxies and models, Earth Planet. Sc. Lett., 349–350, 53–66, doi:10.1016/j.epsl.2012.06.024, 2012.

Huber, M.: Progress in greenhouse climate modelling, in: Reconstructing Earth's Deep-Time Climate, edited by: Linda Ivany, B. H., Paleontological Society, 2012.

Huber, M. and Caballero, R.: The early Eocene equable climate problem revisited, Clim. Past, 7, 603–633, doi:10.5194/cp-7-603-2011, 2011.

Huber, M., Sloan, L. C., and Shellito, C.: Early Paleogene oceans and climate; fully coupled modeling approach using the NCAR CCSM, in: Causes and consequences of globally warm climates in the early Paleogene, edited by: Wing, S. L., Gingerich, P. D., Schmitz, B., and Thomas, E., Geological Society of America (GSA), Boulder, CO, 2003.

Iakovleva, A. I., Brinkhuis, H., and Cavagnetto, C.: Late Palaeocene–Early Eocene dinoflagellate cysts from the Turgay Strait, Kazakhstan; correlations across ancient seaways, Palaeogeogr. Palaeocl., 172, 243–268, doi:10.1016/S0031-0182(01)00300-5, 2001.

Janecek, T. R. and Rea, D. K.: Eolian deposition in the northeast Pacific Ocean: Cenozoic history of atmospheric circu-

lation, Geol. Soc. Am. B., 94, 730–738, doi:10.1130/0016-7606(1983)94<730:editnp>2.0.co;2, 1983.

Jayne, S. R., Laurent, L. C. S., and Gille, S. T.: Connections Between Ocean Bottom Topography and Earth's Climate, Oceanography, 17, 65–74, 2004.

Kaplan, J. O., Bigelow, N. H., Prentice, I. C., Harrison, S. P., Bartlein, P. J., Christensen, T. R., Cramer, W., Matveyeva, N. V., McGuire, A. D., Murray, D. F., Razzhivin, V. Y., Smith, B., Walker, D. A., Anderson, P. M., Andreev, A. A., Brubaker, L. B., Edwards, M. E., and Lozhkin, A. V.: Climate change and Arctic ecosystems: 2. Modeling, paleodata-model comparisons, and future projections, J. Geophys. Res., 108, 8171, doi:10.1029/2002jd002559, 2003.

Kump, L. R. and Pollard, D.: Amplification of Cretaceous Warmth by Biological Cloud Feedbacks, Science, 320, 5873, doi:10.1126/science.1153883, 2008.

Langford, R. P., Wilford, G. E., Truswell, E. M., Totterdell, J. M., Yeung, M., Isem, A. R., Yeates, A. N., Bradshaw, M., Brakel, A. T., Olissoff, S., Cook, P. J., and Strusz, D. L.: Palaeogeographic Atlas of Australia, edited by: Australia, G., Canberra, 2001.

Lawver, L. A., Gahagan, L. M., and Dalziel, I. W. D.: A Different Look at Gateways: Drake Passage and Australia/Antarctica, in: Tectonic, Climatic, and Cryospheric Evolution of the Antarctic Peninsula, American Geophysical Union, 5–33, 2011.

Liu, Z., Pagani, M., Zinniker, D., DeConto, R., Huber, M., Brinkhuis, H., Shah, S. R., Leckie, R. M., and Pearson, A.: Global Cooling During the Eocene-Oligocene Climate Transition, Science, 323, 1187–1190, doi:10.1126/science.1166368, 2009.

Livermore, R., Hillenbrand, C.-D., Meredith, M., and Eagles, G.: Drake Passage and Cenozoic climate: An open and shut case?, Geochem. Geophy. Geosyst., 8, Q01005, doi:10.1029/2005gc001224, 2007.

Lunt, D. J., Valdes, P. J., Jones, T. D., Ridgwell, A., Haywood, A. M., Schmidt, D. N., Marsh, R., and Maslin, M.: CO_2-driven ocean circulation changes as an amplifier of Paleocene-Eocene thermal maximum hydrate destabilization, Geology, 38, 875–878, doi:10.1130/g31184.1, 2010.

Lunt, D. J., Dunkley Jones, T., Heinemann, M., Huber, M., LeGrande, A., Winguth, A., Loptson, C., Marotzke, J., Roberts, C. D., Tindall, J., Valdes, P., and Winguth, C.: A model-data comparison for a multi-model ensemble of early Eocene atmosphere-ocean simulations: EoMIP, Clim. Past, 8, 1717–1736, doi:10.5194/cp-8-1717-2012, 2012.

Lyle, M.: Could early Cenozoic thermohaline circulation have warmed the poles?, Paleoceanography, 12, 161–167, 1997.

Mackensen, A. and Berggren, W. A.: Paleogene benthic foraminifers from the southern Indian Ocean (Kerguelen Plateau): biostratigraphy and paleoecology, Proceedings of the Ocean Drilling Program, Scientific Results, 120, 1992.

Markwick, P. J.: The palaeogeographic and palaeoclimatic significance of climate proxies for data-model comparisons, in: Deep-Time Perspectives on Climate Change: Marrying the Signal from Computer Models and Biological Proxies, edited by: Williams, M., Haywood, A. M., Gregory, J., and Schmidt, D. N., Geological Society Special Publication, 251–312, 2007.

Markwick, P. J. and Valdes, P. J.: Palaeo-digital elevation models for use as boundary conditions in coupled ocean-atmosphere GCM experiments: a Maastrichtian (late Cretaceous) example, Palaeogeogr. Palaeocl., 213, 37–63, 2004.

Micheels, A., Bruch, A. A., Uhl, D., Utescher, T., and Mosbrugger, V.: A Late Miocene climate model simulation with ECHAM4/ML and its quantitative validation with terrestrial proxy data, Palaeogeogr. Palaeocl., 253, 251–270, 2007.

Mix, H. T., Mulch, A., Kent-Corson, M. L., and Chamberlain, C. P.: Cenozoic migration of topography in the North American Cordillera, Geology, 39, 87–90, doi:10.1130/g31450.1, 2011.

Molnar, P., Boos, W. R., and Battisti, D. S.: Orographic Controls on Climate and Paleoclimate of Asia: Thermal and Mechanical Roles for the Tibetan Plateau, Annu. Rev. Earth Pl. Sci., 38, 77–102, doi:10.1146/annurev-earth-040809-152456, 2010.

Morley, R. J.: Cretaceous and Tertiary climate change and the past distribution of megathermal rainforests, in: Tropical Rainforest Responses to Climatic Change, Springer Praxis Books, Springer Berlin Heidelberg, 1–31, 2007.

Müller, R. D., Sdrolias, M., Gaina, C., and Roest, W. R.: Age, spreading rates, and spreading asymmetry of the world's ocean crust, Geochem. Geophy. Geosyst., 9, Q04006, doi:10.1029/2007gc001743, 2008a.

Müller, R. D., Sdrolias, M., Gaina, C., Steinberger, B., and Heine, C.: Long-Term Sea-Level Fluctuations Driven by Ocean Basin Dynamics, Science, 319, 1357–1362, 2008b.

Neale, R. B., Richter, J. H., Conley, A. J., Park, S., Lauritzen, P. H., Gettelman, A., Williamson, D. L., Rasch, P. J., Vavrus, S. J., Taylor, M. A., Collins, W. D., Zhang, M., and Lin, S.-J.: Description of the NCAR Community Atmosphere Model (CAM 4.0) National Center for Atmospheric Research, 2010.

Otto-Bliesner, B. L. and Upchurch, G. R.: Vegetation-induced warming of high-latitude regions during the Late Cretaceous period, Nature (London), 385, 804–807, 1997.

Perch-Nielsen, K., Supko, P. R., Boersma, A., Carlson, R. L., Dinkelman, M. G., Fodor, R. V., Kumar, N., McCoy, F., Thiede, J., and Zimmerman, H. B.: Site 357; Rio Grande Rise, DSDP Deep Sea Drilling Project, 1977.

Phillips, J. D. and Forsyth, D.: Plate Tectonics, Paleomagnetism, and the Opening of the Atlantic, Geol. Soc. Am. B., 83, 1579–1600, doi:10.1130/0016-7606(1972)83[1579:ptpato]2.0.co;2, 1972.

Pollard, D. and DeConto, R. M.: Hysteresis in Cenozoic Antarctic ice-sheet variations, Global Planet. Change, 45, 9–21, 2005.

Polzin, K. L., Toole, J. M., Ledwell, J. R., and Schmitt, R. W.: Spatial Variability of Turbulent Mixing in the Abyssal Ocean, Science, 276, 93–96, doi:10.1126/science.276.5309.93, 1997.

Roberts, C. D., LeGrande, A. N., and Tripati, A. K.: Climate sensitivity to Arctic seaway restriction during the early Paleogene, Earth Planet. Sc. Lett., 286, 576–585, doi:10.1016/j.epsl.2009.07.026, 2009.

Rosenbloom, N., Shields, C., Brady, E. C., Levis, S., and Yeager, S. G.: Using CCSM3 for Paleoclimate Applications, National Center for Atmospheric Research, 2011.

Scher, H. D. and Martin, E. E.: Timing and Climatic Consequences of the Opening of Drake Passage, Science, 312, 428–430, doi:10.1126/science.1120044, 2006.

Schlich, R.: Sites 246 and 247, DSDP Deep Sea Drilling Project, 1974.

Schubert, G. and Sandwell, D.: Crustal volumes of the continents and of oceanic and continental submarine plateaus, Earth Planet. Sc. Lett., 92, 234–246, 1989.

Scotese, C. R. and Golonka, J.: Paleogeographic Atlas, PALEOMAP Progress Report 20-0692, Department of Geology, University of Texas at Arlington, 34, 1992.

Sessa, J. A., Ivany, L. C., Schlossnagle, T. H., Samson, S. D., and Schellenberg, S. A.: The fidelity of oxygen and strontium isotope values from shallow shelf settings: Implications for temperature and age reconstructions, Palaeogeogr. Palaeocl., 342–343, 27–39, doi:10.1016/j.palaeo.2012.04.021, 2012.

Sewall, J. O. and Sloan, L. C.: Come a little bit closer: A high-resolution climate study of the early Paleogene Laramide foreland, Geology, 34, 81–84, doi:10.1130/g22177.1, 2006.

Sewall, J. O., Sloan, L. C., Huber, M., and Wing, S.: Climate sensitivity to changes in land surface characteristics, Global and Planetary Change, 26, 445-465, 2000.

Shellito, C. J. and Sloan, L. C.: Reconstructing a lost Eocene paradise: Part I. Simulating the change in global floral distribution at the initial Eocene thermal maximum, Global Planet. Change, 50, 1–17, 2006a.

Shellito, C. J. and Sloan, L. C.: Reconstructing a lost Eocene Paradise, Part II: On the utility of dynamic global vegetation models in pre-Quaternary climate studies, Global Planet. Change, 50, 18–32, 2006b.

Shellito, C. J., Sloan, L. C., and Huber, M.: Climate model sensitivity to atmospheric CO_2 levels in the Early-Middle Paleogene, Palaeogeogr. Palaeocl., 193, 113–123, 2003.

Shellito, C. J., Lamarque, J.-F., and Sloan, L. C.: Early Eocene Arctic climate sensitivity to pCO_2 and basin geography, Geophys. Res. Lett., 36, doi:10.1029/2009gl037248, 2009.

Simmons, H. L., Jayne, S. R., Laurent, L. C. S., and Weaver, A. J.: Tidally driven mixing in a numerical model of the ocean general circulation, Ocean Model., 6, 245–263, doi:10.1016/S1463-5003(03)00011-8, 2004.

Sloan, L. C.: Equable climates during the early Eocene; significance of regional paleogeography for North American climate, Geology, 22, 881–884, 1994.

Sloan, L. C. and Rea, D. K.: Atmospheric carbon dioxide and early Eocene climate: A general circulation modeling sensitivity study, Palaeogeogr. Palaeocl., 119, 275–292, 1996.

Stein, C. A. and Stein, S.: A model for the global variation in oceanic depth and heat flow with lithospheric age, Nature, 359, 123–129, 1992.

Stickley, C. E., Brinkhuis, H., Schellenberg, S. A., Sluijs, A., Röhl, U., Fuller, M., Grauert, M., Huber, M., Warnaar, J., and Williams, G. L.: Timing and nature of the deepening of the Tasmanian Gateway, Paleoceanography, 19, PA4027, doi:10.1029/2004pa001022, 2004.

Stocker, T., Qin, D., and Platner, G.: Climate Change 2013: The Physical Science Basis, Working Group I Contribution to the Fifth Assessment Report of the Intergovernmental Panel on Climate Change, Summary for Policymakers (IPCC, 2013), 2013.

Strömberg, C. A. E.: Evolution of Grasses and Grassland Ecosystems, Annu. Revi. Earth Pl Sci., 39, 517–544, doi:10.1146/annurev-earth-040809-152402, 2011.

Torsvik, T. H., Carlos, D., Mosar, J., Cocks, L. R. M., and Malme, T. N.: Global reconstructions and North Atlantic paleogeography 440 Ma to recent, BATLAS – Mid Norway plate reconstruction atlas with global and Atlantic perspectives, 18–39, Geological Survey of Norway, 2002.

Utescher, T. and Mosbrugger, V.: Eocene vegetation patterns reconstructed from plant diversity – A global perspective, Palaeogeogr. Palaeocl., 247, 243–271, doi:10.1016/j.palaeo.2006.10.022, 2007.

Vincent, E., Gibson, J. M., and Brun, L.: Paleocene and early Eocene microfacies, benthonic foraminifera, and paleobathymetry of Deep Sea Drilling Project sites 236 and 237, western Indian Ocean, DSDP Deep Sea Drilling Project, 1974.

Vinogradov, A. P.: Atlas of the Lithological-paleogeographical Maps of the USSR, Soviet Union Ministerstvo geologii, Moscow, 1967.

Whittaker, J. M., Goncharov, A., Williams, S. E., Müller, R. D., and Leitchenkov, G.: Global sediment thickness data set updated for the Australian-Antarctic Southern Ocean, Geochem. Geophy. Geosyst., 14, 3297–3305, doi:10.1002/ggge.20181, 2013.

Wilson, D. S., Jamieson, S. S. R., Barrett, P. J., Leitchenkov, G., Gohl, K., and Larter, R. D.: Antarctic topography at the Eocene–Oligocene boundary, Palaeogeogr. Palaeocl., 335–336, 24–34, doi:10.1016/j.palaeo.2011.05.028, 2012.

Winguth, A., Shellito, C., Shields, C., and Winguth, C.: Climate Response at the Paleocene–Eocene Thermal Maximum to Greenhouse Gas Forcing – A Model Study with CCSM3, J. Climate, 23, 2562–2584, doi:10.1175/2009jcli3113.1, 2009.

Wohlfahrt, J., Harrison, S., Braconnot, P., Hewitt, C., Kitoh, A., Mikolajewicz, U., Otto-Bliesner, B., and Weber, S.: Evaluation of coupled ocean–atmosphere simulations of the mid-Holocene using palaeovegetation data from the northern hemisphere extratropics, Clim. Dynam., 31, 871–890, doi:10.1007/s00382-008-0415-5, 2008.

Wolfe, J. A.: Distribution of major vegetational types during the Tertiary, in: Geophysical Monograph, edited by: Sundquist, E. T. and Broecker, W. S., American Geophysical Union, Washington, DC, 357–375, 1985.

Wolfe, J. A., Forest, C. E., and Molnar, P.: Paleobotanical evidence of Eocene and Oligocene paleoaltitudes in midlatitude western North America, Geol. Soc. Am. B., 110, 664–678, doi:10.1130/0016-7606(1998)110<0664:peoeao>2.3.co;2, 1998.

Wright, N., Zahirovic, S., Müller, R. D., and Seton, M.: Towards community-driven paleogeographic reconstructions: integrating open-access paleogeographic and paleobiology data with plate tectonics, Biogeosciences, 10, 1529–1541, doi:10.5194/bg-10-1529-2013, 2013.

Zachos, J. C., Röhl, U., Schellenberg, S. A., Sluijs, A., Hodell, D. A., Kelly, D. C., Thomas, E., Nicolo, M., Raffi, I., Lourens, L. J., McCarren, H., and Kroon, D.: Rapid Acidification of the Ocean During the Paleocene-Eocene Thermal Maximum, Science, 308, 1611–1615, doi:10.1126/science.1109004, 2005.

Ziegler, A. M., Scotese, C. R., and Barrett, S. F.: Mesozoic and Cenozoic Paleogeographic Maps, in: Tidal Friction and the Earth's Rotation II, edited by: Brosche, P. and Sündermann, J., Springer Berlin Heidelberg, 240–252, 1982.

Ziegler, A. M., Rowley, D. B., Lottes, A. L., Sahagian, D. L., Hulver, M. L., and Gierlowski, T. C.: Paleogeographic Interpretation: With an Example From the Mid-Cretaceous, Annu. Rev. Earth Pl. Sci., 13, 385–428, doi:10.1146/annurev.ea.13.050185.002125, 1985.